analytical chemistry

Article

Dual-Emitting Fluorescent Metal-Organic Framework Nanocomposites as a Broad-Range pH sensor for Fluorescence Imaging

Haiyong Chen, Jing Wang, Duoliang Shan, Jing Chen, Shouting Zhang, and Xiaoquan Lu

Anal. Chem., **Just Accepted Manuscript** • DOI: 10.1021/acs.analchem.8b01455 • Publication Date (Web): 04 May 2018

ACS Publications

is published by the American Chemical Society. 1155 Sixteenth Street N.W., Washington, DC 20036

Dual-Emitting Fluorescent Metal-Organic Framework Nanocomposites as a Broad-Range pH sensor for Fluorescence Imaging

Haiyong Chen[a], Jing Wang[a], Duoliang Shan[a], Jing Chen[a], Shouting Zhang[a,b], Xiaoquan Lu[a, b*]

[a] Key Laboratory of Bioelectrochemistry and Environmental Analysis of Gansu Province, College of Chemistry & Chemical Engineering, Northwest Normal University, Lanzhou 730070, P. R. China.

[b] Tianjin Key Laboratory of Molecular Optoelectronic, Department of Chemistry, Tianjin University, Tianjin, 300072, P. R. China.

*Corresponding author: Xiaoquan Lu

E-mail: luxq@tju.edu.cn; luxq@nwnu.edu.cn

Tel: +86 931 7971276/Fax: +86 931 797 1276

ABSTRACT

pH plays an important role in understanding physiological/pathologic processes and abnormal pH is a symbol of many common diseases such as cancer, stroke, and Alzheimer's disease. In this work, an effective dual-emission fluorescent metal-organic framework nanocomposites probe (denoted as RB-PCN) has been constructed for sensitive and broad range detection of pH. RB-PCN was prepared by encapsulating the DBI-PEG-NH_2-functionalized Fe_3O_4 into the Zr-MOFs and then further reacted with rhodamine B isothiocyanates (RBITC). In the RB-PCN, RBITC is capable of sensing changes of pH in the acidic solutions. Zr-MOFs not only enrich the target analyte, but also exhibit a fluorescence response to pH changes in alkaline solutions. Based on above structural and compositional features, RB-PCN could be detected a wide range of pH changes. Importantly, such nanoprobe could "see" the intracellular pH changes by fluorescence confocal imaging as well as "measure" the wider range of pH in actual samples by fluorescence spectra. To the best of our knowledge, this is the first time using MOF based dual-emitting fluorescent nanoprobe for wide range of pH detection.

INTRODUCTION

pH plays an irreplaceable regulatory role in maintaining the stability, the normal morphology and function of cells and organisms.[1-4] Abnormal intracellular pH can affect the cell differentiation and apoptosis,[5,6] muscle contraction,[7] ion transport and internal environment stability,[8-10] causing a series of adverse reactions; even some of the disease also derive from the pH anomaly.[11,12] Therefore, the study of pH changes in living cells is important for revealing the mechanism of cell metabolism and different physiological and pathological processes and intracellular drug delivery process.[13,14] Fluorescence spectroscopy[15-17] is under a unique advantage in detecting pH changes in spatiotemporal distribution, as compared to pH measurement methods such as proton permeable microelectrode,[18] ^{31}P NMR spectroscopy[19] and absorption spectroscopy.[20] Also, fluorescence-based techniques[21] have the advantages of simple operation, fast response, high signal-to-noise ratio, high sensitivity and in most cases without damage to cells. Generally speaking, two kinds of fluorescent pH probes have been exploited, one that is cytoplasmic probes which work in the pH range of 6.8 - 7.4,[22,23] and the other is probes for acidic organelles such as lysosome which work in the pH range of 4.5 - 6.0.[24,25] However, new probes for use in broad-range pH sensors that are highly sensitive and biocompatible are still highly required.

Metal-organic frameworks (MOFs) are kind of porous materials

consisting of metal ions or clusters and organic ligands.[26,27] They are considered to be one of the foremost candidates for sensing materials because of their high specific surface area, multifunctional framework composition and exposed active sites.[28] It is useful to noting that luminescent metal-organic frameworks (LMOFs) have been successfully applied to analytical chemistry.[29-31] As far as we know, there are little pH sensors based on MOFs have been reported: Rocha et al. [32] depicted an Eu-based MOFs which shows linear pH-dependence across the range from 5 - 7.5. Zhou et al. [33] reported that the PCN-224 based on the organic ligand porphyrin was used as pH-dependent fluorescence probe in the range from 1 to 11. However, the PCN-224 makes a significant fluorescence change only under alkaline conditions. RBITC[34,35] is a commonly used pH probe. However, it has only a significant fluorescence response to the acidic medium. We assume that integrating MOFs and RBITC in one system will broaden the scope of the pH.

In this work, for the first time, we developed a dual-emission fluorescent MOFs-based probe for real-time monitoring pH changes over a wide range (Scheme 1 and Figure S1). First, the DBI-PEG-NH_2-functionalized Fe_3O_4 NPs were encapsulated into the ocket-channel frameworks (PCN-224), and then RBITC was modified onto the surface of encapsulated Fe_3O_4 NPs to obtain target probe (denoted as RB-PCN). The resulting core-shell-like RB-PCN exhibits a

single-excitation, dual-emission fluorescence properties, one from organic ligand porphyrin of PCN and the other from the RBITC. Therefore, RB-PCN probe for pH sensing has the following advantages: (1) The RB-PCN probe can be present in the most wide pH solution and exhibit excellent chemical stability in solutions with the pH range from 1 to 11.[36] (2) The porous structure and open channels of PCN allow H^+ to rapidly and freely diffuse to provide a fast response.[37] (3) The covalent conjugation of RBITC on the surface of Fe_3O_4 nanoparticles encapsulated in PMOF prevents dye leaching, thereby eliminating background disturbances caused by dye release during pH testing. As expected, RB-PCN has excellent photostability and is capable of imaging in cells. RB-PCN can be susceptible to pH changes both in the range 1.7 - 7.0 and 7.0 - 11.3, accompanying by different fluorescence changes. Moreover, the resultant RB-PCN can be used for seeing pH changes in living cells as well as measuring pH in real samples.

EXPERIMENTAL SECTION

Materials and Reagents. Pyrrole, methyl p-formylbenzoate, Iron (III) 2,4-pentanedionate, 1-Amino-9-octadecene, Dibenzyl ether, 3,4-dihydroxybenzaldehyde, polyethene glycol (PEG) (M_W=4000) were purchased from Sigma-Aldrich and implemented without further purification. Zirconium Oxychloride Octahydrate ($ZrOCl_2 \cdot 8H_2O$) and

Benzoic Acid were purchased from Aladdin. Meso-tetra-(4-carbomethoxyphenyl) porphyrin (TCPP-OMe), meso-Tetra (4-carboxyphenyl) porphyrin (TCPP), DBI-PEG-NH_2 and Fe_3O_4 NPs were prepared according to the literature with minor modifications. The solution of metal ions ($Mg(NO_3)_2$, $Zn(NO_3)_2$, KCl, $CuCl_2$, NaCl, $Al(NO_3)_3$, $BaCl_2$, $Ni(NO_3)_2$, $Ca(NO_3)_2$, $AgNO_3$; Na_2SO_4, $NaNO_3$, Na_2HPO_4, NaH_2PO_4, Na_2SO_3, Na_2CO_3, CH_3COONa, $NaHCO_3$, NaI, NaBr, Glucose, L-cysteine, L-glutamic acid, Ascorbic Acid) were dissolved in ultrapure water. TCPP was synthesized according to published methods with minor modifications.[31-33] Fe_3O_4-DBI-PEG-NH_2 and Fe_3O_4-DBI-PEG-NH_2. were synthesized according to the previous method.[38]

Apparatus. Field-emission scanning electron microscope (FE-SEM, FEI, Sirion 200) and Transmission electron microscopy (TEM, Philips EM 420 (120 kV)) were utilized to confirm the morphology of RB-PCN. Bruker AXS D8-Advanced diffractometer with Cu Kα radiation (λ=1.5418Å) was used to record X-ray powder diffraction (XRD) patterns of the nanomaterials. FT-IR characterization was recorded on a Bruker Vertex 70 FT-IR spectrometer. UV-vis absorbance measurements were performed on Shimadzu UV-1750. Fluorescence spectroscopy was performed on a Shimadzu RF-5301 spectrofluoro Photo-meter. Fluorescence images of cell imaging were made using a Zeiss Leica

inverted epifluorescence/reflectance laser scanning confocal microscope.

Synthesis of Meso-tetra-(4-carbomethoxyphenyl) porphyrin (TCPP-OMe). Methyl p-formylbenzoate (16.5 g, 0.1 mol) was dissolved in propionic acid (250 mL) in a 500 mL three-necked flask and heated to 140 ℃ with stirring. Pyrrole (6.7 mL, 0.1 mol) dissolved in 30 mL of propionic acid was then added drop wise over 30 min and the solution was refluxed for 2 h. After the reaction, 150 mL of ethanol was added to the mixture which cooled to room temperature. Finally, the precipitates were collected by suction-filtration and washed with methanol, ethyl acetate and THF, respectively. After drying in an oven for 12 h, purple solid was obtained.

Synthesis of Meso-Tetra (4-carboxyphenyl) porphyrin (TCPP). In a 250-mL single-necked flask, the obtained TCPP-OMe (0.164 g, 0.2 mmol) was stirred in 150 ml mixture of THF and MeOH (v: v = 2: 1), to which a solution of 12 ml NaOH (40%) was introduced. The mixture as refluxed for 2 h at 40 ℃. After the reaction, the solution was adjusted to pH 4 - 5 with hydrochloric acid. The solution was then extracted 2 - 3 times with a mixed solvent of THF and CH_2Cl_2 (v: v = 1 : 1), and the organic phase was distilled off to remove the solvent. Then the product was placed in an oven at 40 ℃ for dry, and violet purple red target products was obtained.

Synthesis of Fe_3O_4 nanoparticles (NPs). The synthesis of Fe_3O_4 NPs is based on the literature method.[38] Firstly, acetylacetonate (2 mmol) was

dissolved in a mixed solution of oleylamine (10 mL) and dibenzyl ether (10 mL), and the reaction was carried out with nitrogen 120 ℃ for 1 h. After heating to 300 ℃ and keeping at this temperature for 2 h, the reaction mixture was cooled to room temperature. The Fe_3O_4 NPs were precipitated by adding ethanol (40 mL) and collected by centrifugation. The prepared Fe_3O_4 NPs were redispersed in n-hexane and preserved at low temperature.

Synthesis of Fe_3O_4 NPs@PCN-224.[39-42] In a typical synthesis, 30 mg $ZrOCl_2 \cdot 8H_2O$, 10 mg TCPP and 300 mg benzoic acid were dissolved in 6 mL DMF and sonicated for 10 min. Then, 0.8 mg Fe_3O_4-DBI-PEG-NH_2 was added to the above solution. The mixture was sonicated for 10 min before heating in oven at 120 ℃ for 24 h. After cooling to room temperature, the obtained precipitate was centrifuged (5000 rpm, 3 min) and washed three times with DMF. Finally, by soaked with acetone, the solid was centrifuged and dried in a vacuum oven for further use.

Post-synthetic loading of rhodamineisothiocyanate (RB-PCN). 1 mL anhydrous ethanol solution of RBITC (1 mg/mL) was added to 2 mL anhydrous ethanol solution with 4 mg Fe_3O_4 NPs@PCN-224. After the mixture stirred at room temperature in the dark for 24 h to afford RB-PCN, the product was collected by centrifugation at 5000 rpm and washed with ethanol.

Spectral Measurements. The stock solution of RB-PCN was prepared

with ultrapure water. In the pH titration experiment, the stock solution was diluted to 100 mg/L with ultrapure water, and the pH of the solution required was adjusted by adding a certain amount of NaOH or HC1. Then, the resulting solution was transferred to a quartz cell to acquire fluorescence spectrum with λex = 520 nm.

In the study of the reversibility of RB-PCN, the pH of the RB-PCN (100 mg/L) solution was converted between 4.0 and 11.0 with 1 M NaOH or HCl. The interference of other ions /bio-molecules (Mg^{2+}, Zn^{2+} , K^{+}, Cu^{2+}, Na^{+}, Al^{3+}, Ba^{2+}, Ni^{2+}, Ca^{2+}, Ag^{+}; SO_4^{2-}, $H_2PO_4^{-}$, HCO_3^{-}, SO_3^{2-}, HPO_4^{2-}, NO_3^{-}, CO_3^{2-}, Cl^{-}, AcO^{-}, Br^{-}, I^{-}, S^{2-}; Glucose, L-cysteine, L-glutamic acid, Ascorbic acid) to the fluorescence intensity of RB-PCN was detected at pH 6.9 and 11.0, respectively.

Cytotoxicity Assay. The evaluation about in vitro cytotoxicity of probe RB-PCN performed by MTT assay in the HeLa cells incubated with the probe RB-PCN. Cells were seeded into a 96-well plate (5×10^4 cells/well) containing 10% FBS (fetal bovine serum) in DMEM (Dulbecco's modified eagle's medium) under 5% CO_2 at 37 °C for 24 h. The cells were then incubated with RB-PCN for 24 h and 48 h at 37 ℃ under 5% CO_2, respectively, where the concentrations of RB-PCN were 20, 40, 60, 80, 100, 120 mg/L in DMEN. Cells in a culture medium without RB-PCN were used as a control. Next, MTT (20 μL/well, 5 mg/mL) was added to each well plate and the plate was incubated at 37 ℃ and 5% CO_2 for 4 h.

After adding 100 μL/well DMSO (dimethylsulfoxide), the plate of cells was permitted to maintain 15 min at 37 °C. Finally, the optical density at 492 nm (A_{492}) of the extraction liquid was detected using a microplate reader.

Flow cytometry assay. Cells were treated as described above. Before measurement by flow cytometry, cells were scraped off gently and collected into a clean centrifuge tube. Then, cells were centrifuged (800 rpm, room temperature, 3 min). After removing the supernatant, 1 mL PBS was slowly added to resuspend the cell pellet. Finally, cells were analyzed on a Beckman flow cytometer equipped with a 488 nm Ar laser, and fluorescence was collected by PE channel.

Fluorescence confocal imaging. The HeLa cells were seeded into a 6-well plate (5×10^5 cells/well) containing 10% FBS in DMEM (Dulbecco's modified eagle's medium) under 5% CO_2 at 37 °C for 24 h. The cells were then incubated with RB-PCN (final concentration of 40 mg/L) and the lysosome dye LysoBlue (final concentration of 1 μM, KeyGEM, China) or the cytoplasm tracker CMAC (7-amino-4-chloro-O-methyl coumarin, final concentration of 1 μM, Invitrogen, United States) for 1 h under standard culture conditions. Then the cells were washed with PBS three times and incubated with PBS buffer solutions at pH 5.0, 7.0 or 8.0 for 20 min containing 100 μM Nigericin,[41] and observed by confocal microscopy (λ_{ex}=360 nm and λ_{em}=

460 nm for LysoBlue or CMAC; λ_{ex}=520 nm and λ_{em}= 575 nm or 641 nm for RB-PCN, Olympus, Japan).

Analysis of real Sample. We use the Yellow River (Lanzhou, China) and tap water as actual water samples for testing. The samples were centrifuged at 13 000 rpm for 3 min and filtered through a membrane to eliminate impurities, and then used to prepare solutions at different pH values.

RESULTS AND DISCUSSION

Characterization of RB-PCN. Figures 1a shows SEM images of RB-PCN. It can be seen that the resultant RB-PCN still maintained uniform cube sphere crystals with an average size of 330 nm (Figure S2), which is maintained the morphology of PCN-224 (Figure S3). Transmission electron microscopy (TEM) image of RB-PCN revealed their well-defined micro-structure (Figure 1b, Figure S4). As shown in Figure S5, it can be seen that RB-PCN contains Fe, Zr, Cl, O elements, indicating the successful preparation of RB-PCN. According to the literature,[43] the similar powder X-ray diffraction (PXRD) curves show that the crystalline and structural integrity of PCN-224 is not destroyed after encapsulation of Fe_3O_4 nanoparticles (Figure 1c). The peaks observed at 30.1°, 35.3°, 42.9°, 53.5°, 57.0°, and 62.5° were assigned to (220), (311), (400), (422), (511) and (440) planes of cubic structure of

Fe_3O_4 crystal (JCPDS No.75-1609). The simultaneous existence of the characteristic peaks of Fe_3O_4 NPs[38] and PCN-224[43,44] in its PXRD pattern indicates the successful formation of RB-PCN nanocomposites. FTIR demonstrated that the RB-PCN was comprised of Fe_3O_4-DBA-PEG-NH_2, PCN-224 and RBITC (Figure S6).

Identification performance of RB-PCN in different pH. Firstly, we tested the UV-vis absorption spectra of RB-PCN in different pH solution. Figure 2 shows the absorption spectra at pH 3.0, 7.0 and 10.0, respectively. In the acidic condition, the characteristic absorption peak of RBITC appeared at 450 nm, and this peak position appeared blue shift and finally disappeared with the increase of pH to alkaline. When the pH arrived to 10, the characteristic absorption peak of organic ligand porphyrin at 420 nm was appeared. Also, we observed that RB-PCN undergoes a slight change from pink to yellow-green with pH increasing in aqueous solution.

Moreover, we carried out standard fluorescence pH titration analysis of the aqueous solution of RB-PCN at a concentration of 100 mg/L. Figure 3a shows the fluorescence emission spectra under acidic conditions. RB-PCN has weak fluorescence intensity at 575 nm at neutral solution. With the decrease of pH value, the fluorescence intensity of RB-PCN at 575 nm gradually increased, which was result of the ring-opening effect of RBITC[34] (Scheme 2a). In the pH range of 1.7 - 7.0, the relationship

between pH (X axis) and fluorescence intensity (Y axis) can be described by a perfect linear regression relationship with $R^2 = 0.9952$ (Figure 3b). The linear regression relationship equation is as follows: pH=17.099 - 0.079y (y=Fluorescence intensity). Any sample of pH range under acidic conditions can be calculated by this formula. We still choose 520 nm as the excitation wavelength under alkaline conditions. Under alkaline conditions, the fluorescence emission intensity of RB-PCN at 641nm gradually increases with the increase of pH (Figure 3c). The enhancement of the fluorescence intensity is due to the deprotonation of the imino groups of the porphyrin ligand in the PCN-224 framework under alkaline conditions[31] (Scheme 2b). This is of great significance for studying the pH change in the chemical system.

Figure 4 indicates the reversibility of the probe in the acidic range and the alkaline range, respectively. After four cycles, the probe still works well, indicating that RB-PCN is a highly reversible probe for sensing pH. At the same time, it was proved that RB-PCN had excellent stability by detecting the change of fluorescence intensity at pH 4.0, 7.0 and 11.0 (Figure 4, Figure S7).

To further explore the performance of RB-PCN, we selected some metal ions, anions and bio-molecules as interference objects to explore the anti-interference ability of RB-PCN in the complex environment. The measurement was carried out by adding separate interfering ions at a

concentration of 100 μM to the RB-PCN solution at pH 7.0 and 11.0. As shown in Figure 5 and Figure S8, the addition of interference reagents did not significantly affect the fluorescence intensity at 575 nm and 641 nm. The results indicated the high selectivity and selectivity of RB-PCN to pH.

Cell Toxicity and Fluorescence confocal imaging. HeLa cells were used to evaluate the toxicity of RB-PCN probe. As shown in Figure S9, RB-PCN presented relatively low toxicity to the cells at different times. When the incubation time of RB-PCN reached to 48 h, the cell survival rate was higher than 70%, which indicated that RB-PCN had low toxicity and could be employed in fluorescence imaging in vitro. To verify the probe RB-PCN located into cells, flow cytometry analysis was performed to observe the change of fluorescence inside cells. As shown in Figure S10, significant enhancement of fluorescence emission was observed after incubating with RB-PCN, suggesting the probe RB-PCN can be used for cell imaging.

Next, we explored to use RB-PCN to sense the pH fluctuation in cells by confocal microscopy. The HeLa cells were incubated with RB-PCN (40 mg/L) for 1 h, and then treated by PBS at pH 5.0 (Figure 6a-e), 7.0 (Figure 6f-j), and 8.0 (Figure 6k-o) for 20 min in the presence of 100 μM Nigericin. As shown in Figure 6b, at pH 5.0 the cells mainly emitted the strong bright yellow fluorescence. When the pH increased to 7.0, yellow

fluorescence was dimmed out and red fluorescence enhanced. When the pH arrived at 8.0, the cells mainly emitted the strong red fluorescence. Moreover, both the red and the bright yellow fluorescence of RB-PCN could overlap the fluorescence of the lysosome tracker dye LysoBlue, indicating that RB-PCN was localized in the lysosome (Figure 6). These results showed that RB-PCN is suitable for fluorescence imaging to reflect lysosome pH changes in living cells.

Further, we stained HeLa cells with RB-PCN and the cytoplasm tracker dye CMAC, and found that RB-PCN can image in the cytoplasm (Figure 7). The changes in fluorescence at different pH values are consistent with changes in lysosomes. In addition, the red and bright yellow fluorescence of RB-PCN can overlap with that of the cytoplasmic tracking dye CMAC. Simultaneously, by semi-quantifaction by Image J software revealed that the red and yellow fluorescence intensity had turn-on and turn-off behaviors, respectively (Figure S11). The statistical significance results showed that RBITC channel at pH 5.0 (R=20.9±2.52) exhibited an obvious difference from that at pH 7.0(5.21±2.01, $p < 0.01$). And the PCN channel at pH 7.0 (6.67±3.15) also exhibited an obvious difference from that at pH 8.0 (9.46±0.62, $p < 0.05$). In short, RB-PCN has the ideal sensitivity for detecting cell pH.

The application of the RB-PCN in the actual water sample detection. In order to further assess the anti-interference ability of

fluorescent probes, we selected the Yellow River water, tap water and deionized water to prepare the solutions with different pH values, and evaluated the differences in the detection of different water samples. As shown in the Figure 8, the fluorescence intensity of the solution gradually increased with the decrease of pH value in tap water, Yellow River water and deionized water. Moreover, the fluorescence intensity values of RB-PCN in the three water samples were the same as those of the pH value, and no significant difference was observed. And fluorescence intensity was linear with pH. It is shown that the detection system is the same as the result of deionized water detection in laboratory conditions, and can effectively eliminate the interference of coexisting ions, organic pollutants and so on, and prove the excellent selectivity of RB-PCN.

Conclusion

In summary, we successfully prepared a dual-emission fluorescent MOFs-based nanoprobe (RB-PCN) for rapid and ultrasensitive detection of pH in abroad range from 1 - 11. This nanocomposites was synthesized by encapsulating the DBI-PEG-NH_2-functionalized Fe_3O_4 NPs into the PCN-224 and then further reacted with RBITC, in which the RBITC was modified on the surface of Fe_3O_4 NPs. The resulting core-shell-like RB-PCN exhibited two emissions at 575 nm for RBITC in response to the acidic range and 641 nm for PCN-224 in response to the alkaline

range under the same excitation wavelength. Importantly, PCN-224 shell as a protective layer can not only prevent the aggregation of nanoparticles, but also enrich the target analyte, thereby amplifying the fluorescence signal. Moreover, the resultant RB-PCN probe could "see" the pH change in in living cells and "measure" the pH values in actual water sample. This work opens up a new strategy to develop a dual emission fluorescence MOFs based- probes for wide range of pH detection.

ASSOCIATED CONTENT

Supporting Information

Synthetic route of RB-PCN and Figures S1-S11. This material is available free of charge via the Internet at http://pubs.acs.org.

Acknowledgments

Thanks a lot to Prof. Wujian Miao worked in the University of Southern Mississippi, Prof. Chunyang Zhang worked in Shenzhen advanced institute of science and technology, Prof. Baodui Wang worked in the University of Lanzhou, associate Prof. Qilin Yu worked in Nankai University and associate Prof. Yao Meng worked in Northwestern Polytechnical University for their kind discussion.

This work was supported by Natural Science Foundation of China (Grant Nos. 21575115, 21327005, 21705117); the Program for Chang Jiang Scholars and Innovative Research Team, Ministry of Education, China (Grant No. IRT-16R61) and the Program of Gansu Provincial Higher Education Research Project (Grant No. 2017-D-01).

REFERENCE

(1) Izumi, H.; Torigoe, T.; Ishiguchi, H.; Uramoto, H.; Yoshida, Y.; Tanabe, M.; Ise, T.; Murakami, T.; Yoshida, T.; Nomoto, M.; Kohno, K. *Cancer Treatment Reviews*. **2003**, pp 541-549.

(2) Chesler, M.; Brien, J. O.; Zappala, A.; Cicirata, F.; Barrio, L. C. *Brain* **2008**, 1183-1221.

(3) Paradiso, A. M.; Tsien, R. Y.; Machen, T. E. *Nature* **1987**, *325* (6103), 447-450.

(4) Yue, Y.; Huo, F.; Lee, S.; Yin, C.; Yoon, J. *Analyst* **2017**, *142* (1), 30-41.

(5) Kennedy, R. T.; Huang, L.; Aspinwall, C. A. *J. Am. Chem. Soc.* **1996**, *118* (7), 1795-1796.

(6) Martínez-Zaguilán, R.; Chinnock, B. F.; Wald-Hopkins, S.; Bernas, M.; Way, D.; Weinand, M.; Witte, M. H.; Gillies, R. J. *Cell. Physiol. Biochem.* **1996**, *6* (3), 169-184.

(7) Hetzel, F. W.; Chopp, M. *Radiat. Res.* **1990**, *122* (3), 229-233.

(8) Casey, J. R.; Grinstein, S.; Orlowski, J. *Nat. Rev. Mol. Cell Biol.* **2010**, *11* (1), 50-61.

(9) Donoso, P.; Beltrán, M.; Hidalgo, C. *Biochemistry* **1996**, *35* (41), 13419-13425.

(10) Walker, N. M.; Simpson, J. E.; Levitt, R. C.; Boyle, K. T.; Clarke, L. L. *J. Pharmacol. Exp. Ther.* **2006**, *317* (1), 275-283.

(11) Schindler, M.; Grabski, S.; Hoff, E.; Simon, S. M. *Biochemistry* **1996**, *35* (9), 2811-2817.

(12) Davies, T. A.; Fine, R. E.; Johnson, R. J.; Levesque, C. A.; Rathbun, W. H.; Seetoo, K. F.; Smith, S. J.; Strohmeier, G.; Volicer, L.; Delva, L.; . *Biochem.Biophys.Res.Commun.* **1993**, *194* (0006–291X), 537-543.

(13) Du, J. Z.; Du, X. J.; Mao, C. Q.; Wang, J. *J. Am. Chem. Soc.* **2011**, *133* (44), 17560-17563.

(14) Fukuda, T.; Ewan, L.; Bauer, M.; Mattaliano, R. J.; Zaal, K.; Ralston, E.; Plotz, P. H.; Raben, N. *Ann. Neurol.* **2006**, *59* (4), 700-708.

(15) Wu, Y. X.; Zhang, X. B.; Li, J. Bin; Zhang, C. C.; Liang, H.; Mao, G. J.; Zhou, L. Y.; Tan, W.; Yu, R. Q. *Anal. Chem.* **2014**, *86* (20), 10389-10396.

(16) Charier, S.; Ruel, O.; Baudin, J. B.; Alcor, D.; Allemand, J. F.; Meglio, A.; Jullien, L. *Angew. Chemie - Int. Ed.* **2004**, *43* (36), 4785-4788.

(17) Su, M.; Liu, Y.; Ma, H.; Ma, Q.; Wang, Z.; Yang, J.; Wang, M. *Chem. Commun.* **2001**, 11, 960-961.

(18) Spudich, J. L.; Koshland, D. E. J. *Nature* **1976**, *262*, 467-471.

(19) Hesse, S. J. A.; Ruijter, G. J. G.; Dijkema, C.; Visser, J. *J. Biotechnol.* **2000**, *77* (1), 5-15.

(20) Zhang, R. G.; Kelsen, S. G.; LaManna, J. C. *J. Appl. Physiol.* **1990**, *68* (3), 1101-1106.

(21) Gong, Y. J.; Zhang, X. B.; Chen, Z.; Yuan, Y.; Jin, Z.; Mei, L.; Zhang, J.; Tan, W.; Shen, G. L.; Yu, R. Q. *Analyst* **2012**, *137* (4), 932-938.

(22) Sun, K. M.; McLaughlin, C. K.; Lantero, D. R.; Manderville, R. A. *J. Am. Chem. Soc.* **2007**, *129* (7), 1894-1895.

(23) Pal, R.; Parker, D. *Chem. Commun.* **2007**, 474-476.

(24) Li, G.; Zhu, D.; Xue, L.; Jiang, H. *Org. Lett.* **2013**, *15* (19), 5020-5023.

(25) Galindo, F.; Burguete, M. I.; Vigara, L.; Luis, S. V.; Kabir, N.; Gavrilovic, J.; Russell, D. A. *Angew. Chemie - Int. Ed.* **2005**, *44* (40), 6504-6508.

(26) Férey, G. *Chem. Soc. Rev.* **2008**, *37* (1), 191-214.

(27) Li, B.; Wen, H. M.; Cui, Y.; Zhou, W.; Qian, G.; Chen, B. *Adv. Mater.* **2016**, *28* (40), 8819–8860.

(28) Yang, C. X.; Ren, H. B.; Yan, X. P. *Anal. Chem.* **2013**, *85* (15), 7441-7446.

(29) Zhang, X.; Jiang, K.; He, H.; Yue, D.; Zhao, D.; Cui, Y.; Yang, Y.; Qian, G. *Sensors Actuators, B Chem.* **2018**, *254*, 1069-1077.

(30) Yin, H. Q.; Yang, J. C.; Yin X. B. *Anal. Chem.*, **2017**, *89* (24), 13434–13440.

(31) Yang, Z. R.; Wang, M. M.; Wang, X. S.; Yin X. B. *Anal. Chem.*, **2017**, *89* (3), 1930-1936.

(32) Harbuzaru, B. V.; Corma, A.; Rey, F.; Jordá, J. L.; Ananias, D.; Carlos, L. D.; Rocha, J. *Angew. Chemie - Int. Ed.* **2009**, *48* (35), 6476-6479.

(33) Jiang, H. L.; Feng, D.; Wang, K.; Gu, Z. Y.; Wei, Z.; Chen, Y. P.; Zhou, H. C. *J. Am. Chem. Soc.* **2013**, *135* (37), 13934-13938.

(34) Chen, X.; Pradhan, T.; Wang, F.; Kim, J. S.; Yoon, J. *Chem. Rev.* **2012**, *112* (3), 1910-1956.

(35) Wu, Y. X.; Li, J. B.; Liang, L. H.; Lu, D. Q.; Zhang, J.; Mao, G. J.; Zhou, L. Y.; Zhang, X. B.; Tan, W.; Shen, G. L.; Yu, R. Q. *Chem. Commun.*. **2014**, *50*, 2040-2042.

(36) Zheng, H.; Zhan, X. Q.; Bian, Q. N.; Zhang, X. J. *Chem. Commun.* **2013**, *49* (5), 429-447.

(37) Rowsell, J. L. C.; Yaghi, O. M. *Angew. Chemie - Int. Ed.* 2005, 4670-4679.

(38) Wang, B.; Hai, J.; Liu, Z.; Wang, Q.; Yang, Z.; Sun, S. *Angew. Chemie - Int. Ed.* **2010**, *49* (27), 4576-4579.

(39) Zhang, H.; Li, Y. H.; Chen, Y.; Wang, M. M.; Wang, X. S.; Yin, X. B. *Sci. Rep.* **2017**, *7*, 44153.

(40) Zhao, M.; Deng, K.; He, L.; Liu, Y.; Li, G.; Zhao, H.; Tang, Z. *J. Am. Chem. Soc.* **2014**, *136* (5), 1738-1741.

(41) Liu, Y.; Tang, Z. *Adv. Mater.* **2013**, *25* (40), 5819-5825.

(42) Park, J.; Jiang, Q.; Feng, D.; Mao, L.; Zhou, H. C. *J. Am. Chem. Soc.* **2016**, *138* (10), 3518-3525.

(43) Feng, D.; Chung, W. C.; Wei, Z.; Gu, Z. Y.; Jiang, H. L.; Chen, Y. P.; Darensbourg, D. J.; Zhou, H. C. *J. Am. Chem. Soc.* **2013**, *135* (45), 17105-17110.

(44) Yang, J.; Wang, Z.; Li, Y.; Zhuang, Q.; Gu, J. *Chem. Mater.* **2016**, *28* (8), 2652-2658.

Figures

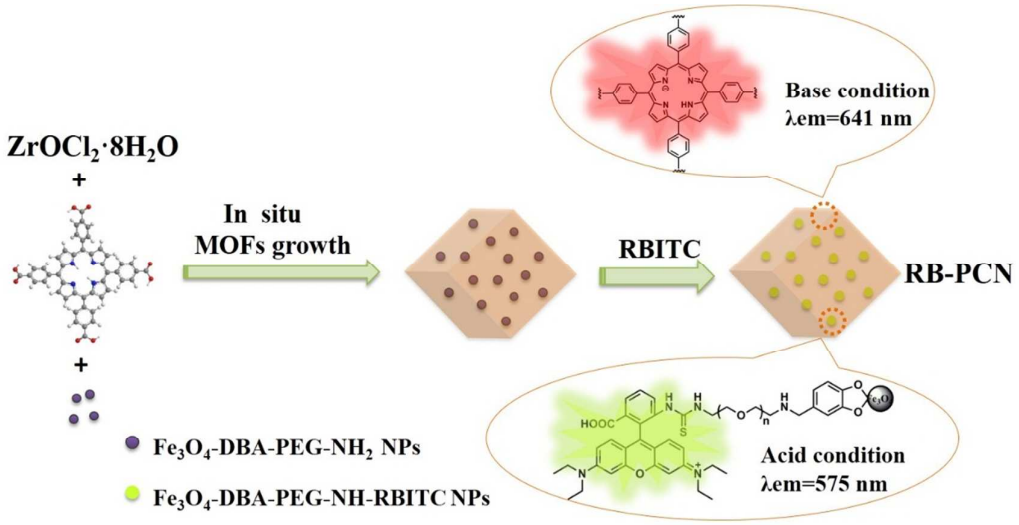

Scheme 1. Design Strategy and Fluorescence Changes of RB-PCN upon pH Variation.

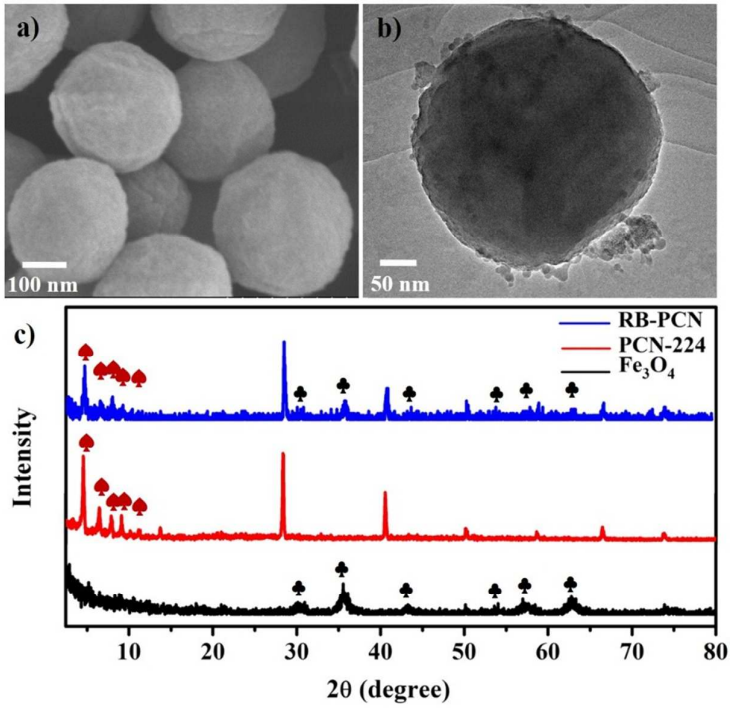

Figure 1. (a) SEM images of RB-PCN, (b) TEM images of RB-PCN, (c) PXRD patterns of

synthesized RB-PCN(blue), PCN-224(red), Fe_3O_4(black).

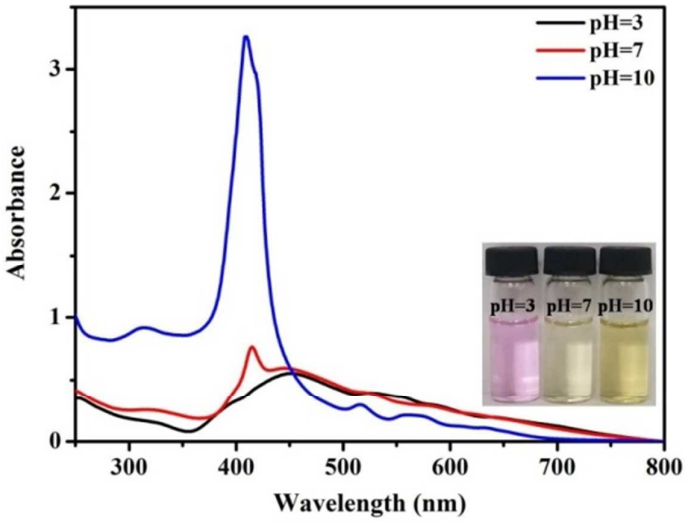

Figure 2. UV-vis absorption spectra of RB-PCN in aqueous solutions with different pH values.

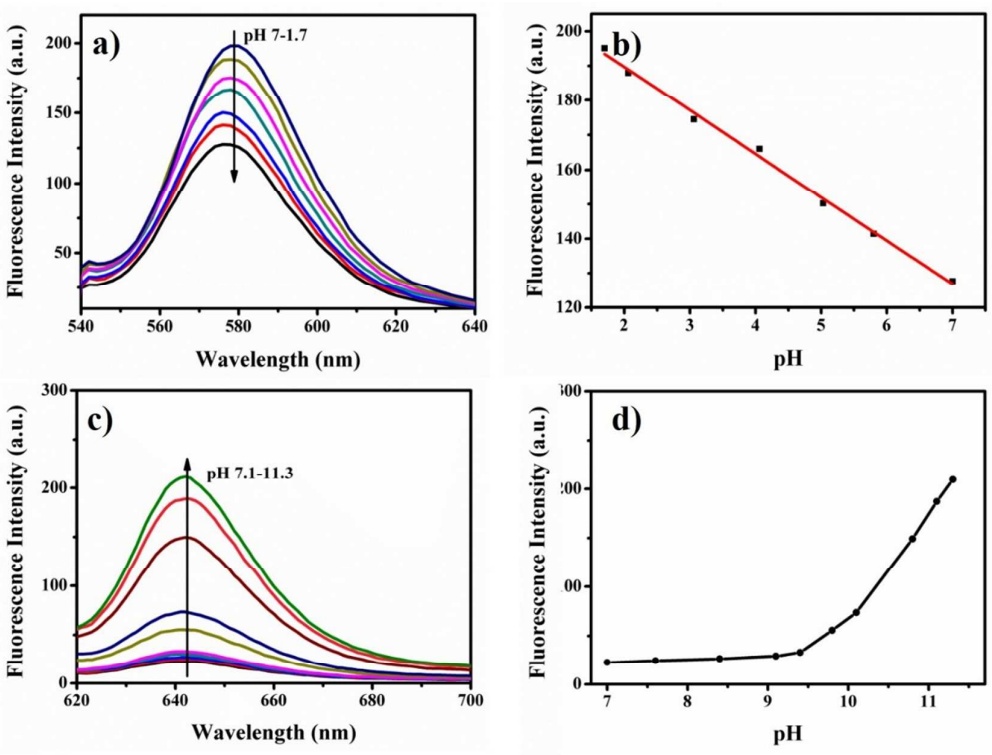

Figure 3. (a) Fluorescence spectra (λex = 520 nm) of the RB-PCN with 100 mg/L in acidic aqueous solutions. (b) Linear relationship of the fluorescence intensity (I575 nm) versus pH values. (c) Fluorescence spectra (λex = 520 nm) of the RB-PCN with 100mg/L in basic aqueous solutions.

(d) Fluorescence intensity (I641 nm) versus pH values.

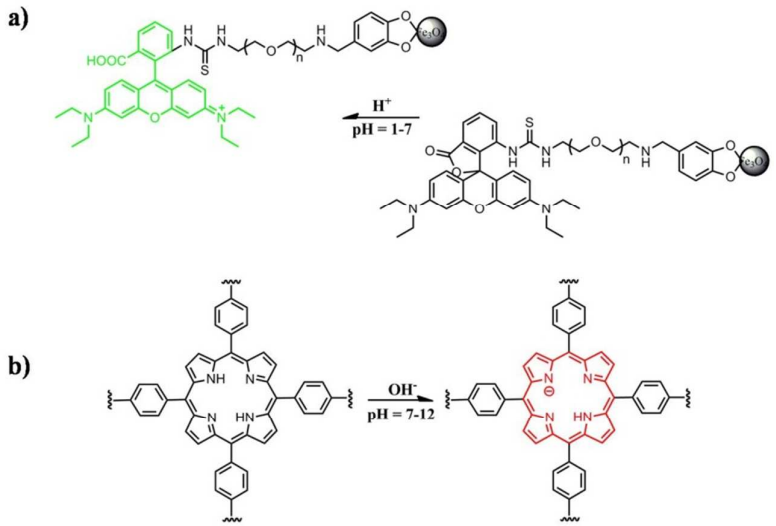

Scheme 2. Proposed sensing mechanism of RB-PCN. (a) Open ring of rhodamine B under acidic conditions. (b) Protonation processes of porphyrin involved in RB-PCN framework.

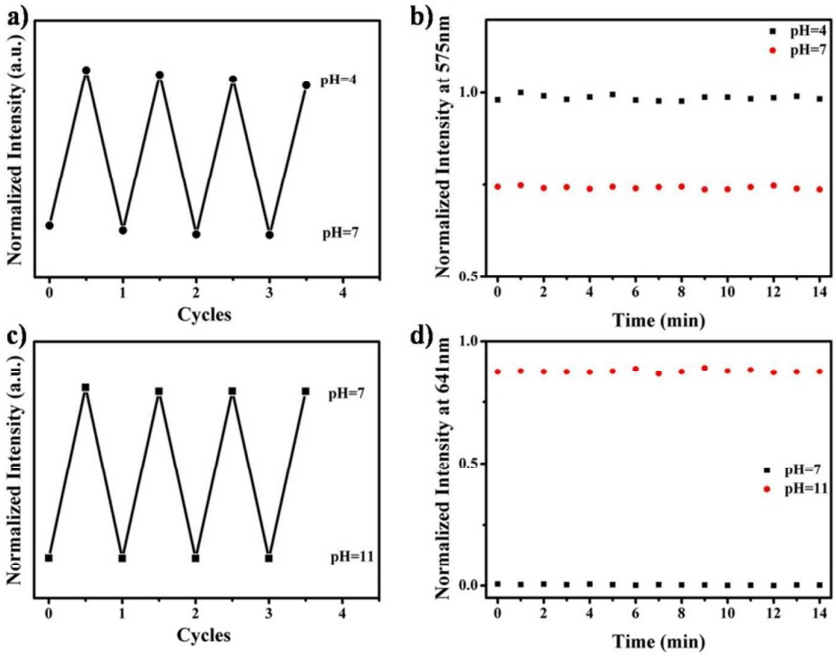

Figure 4. (a) The fluorescence reversibility of RB-PCN (100 mg/L) in aqueous solutions between pH 7.0 and 4.0 at 575 nm. (b) When the pH value is 4.0 and 7.0, the fluorescence intensity of RB-PCN changes with time. The fluorescence reversibility study (c) and the time courses of

fluorescence intensity at 641 nm (d).

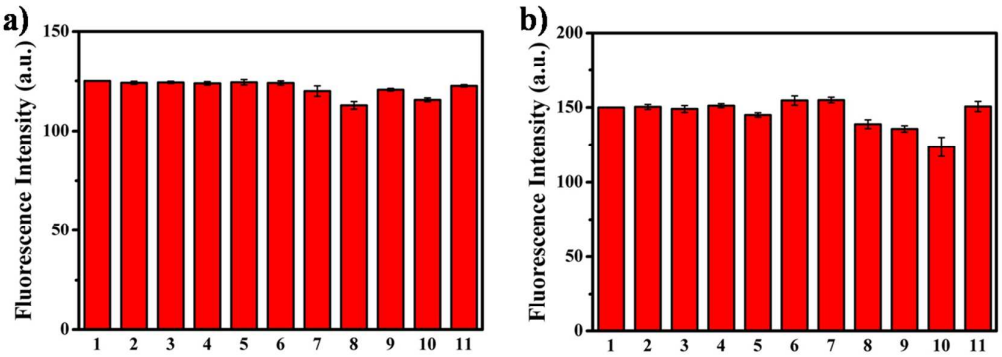

Figure 5. (a) Relative fluorescence intensity changes at 575 nm of 100mg/L RB-PCN in the presence of different metal ions at pH 7.0. (b) Relative fluorescence intensity changes at 641 nm of 100 mg/L RB-PCN in the presence of different metal ions at pH 11.0. 1, blank ; 2, Mg^{2+}; 3, Zn^{2+}; 4, K^{+}; 5, Cu^{2+}; 6, Na^{+}; 7, Al^{3+}; 8, Ba^{2+} 9, Ni^{2+}; 10, Ca^{2+}; 11, Ag^{+}. λex = 520 nm. Error bars are ± s.d.

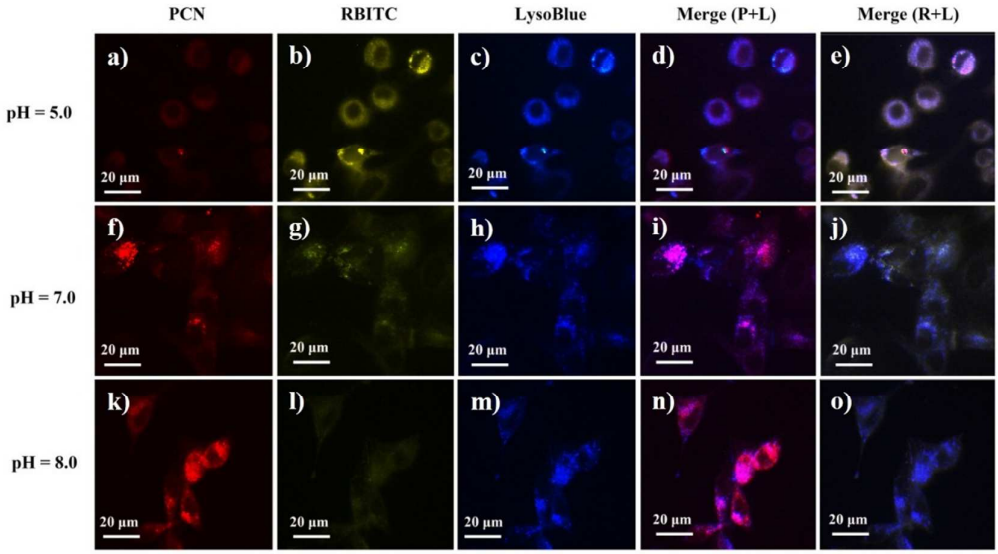

Figure 6. Fluorescence images of HeLa cells after incubation with RB-PCN and LysoBlue (lysosome dye) at different pH (5.0, 7.0 and 8.0). The cells were then observed by confocal microscopy (λ_{ex}=360 nm and λ_{em}= 460 nm for LysoBlue; λ_{ex}=520 nm and λ_{em}= 575 nm or 641 nm for RB-PCN). Merge (P+L), the merging image of PCN and LysoBlue; Merge (R+L), the merging image of RBITC and LysoBlue.

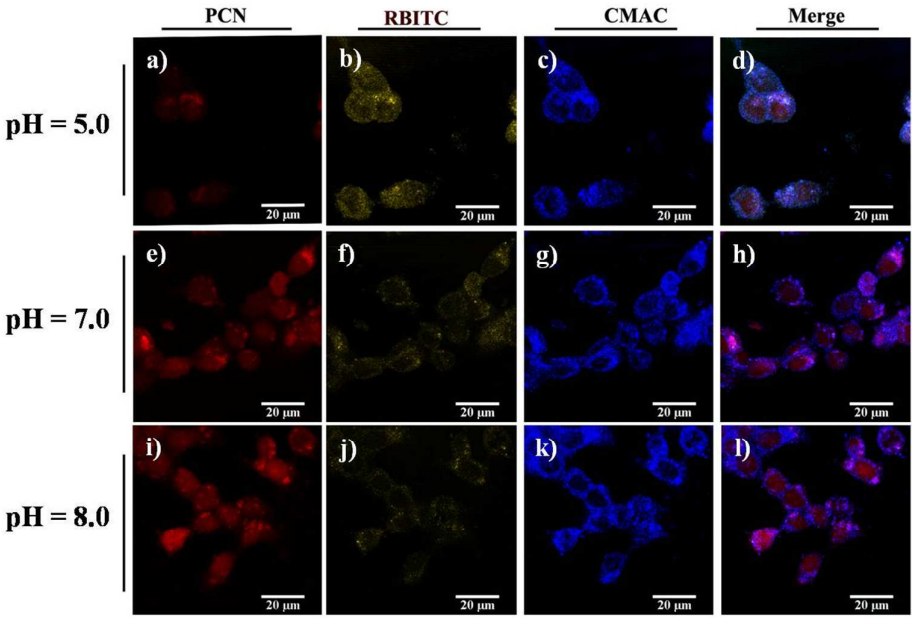

Figure 7. Confocal fluorescence images of HeLa cells after incubation with RB-PCN at different pH (5.0 (a-d), 7.0 (c-h) and 8.0 (i-l)). HeLa cells were stained with the Cell Tracker Blue CMAC (7-amino-4-chlor-omethylcoumarin). The images in the first row and second row were collected in the ranges of 620-660 nm and 540-580 nm, respectively. The images in the fourth row were the merged ones of PCN, RBITC and CMAC channels.

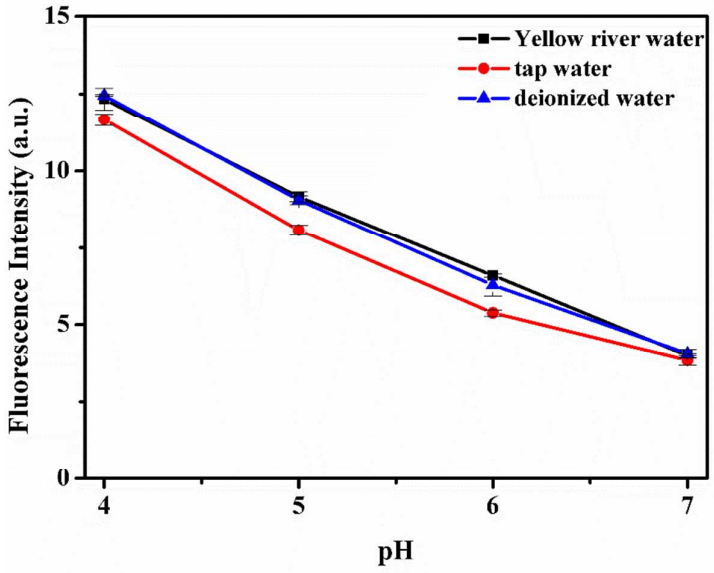

Figure 8. Fluorescence intensity of RB-PCN solution in different water samples with different

pH

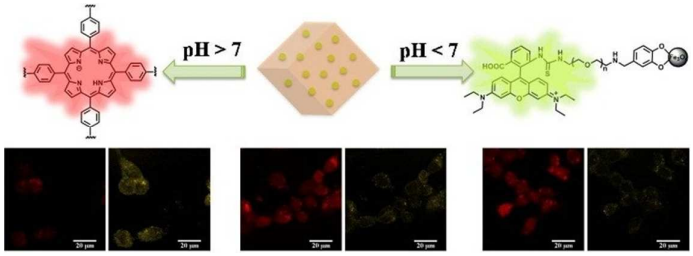

for TOC only